This is the peer reviewd version of the followng article:

01/05/2024 13:53

(Article begins on next page)

THE JOURNAL OF PHYSICAL CHEMISTRY C

Article

Doping of III−V Arsenide and Phosphide Wurtzite Semiconductors

Giacomo Giorgi,[∇] Michele Amato,[∇] Stefano Ossicini, Xavier Cartoixà, Enric Canadell,*
and Riccardo Rurali*

Cite This: https://dx.doi.org/10.1021/acs.jpcc.0c09391

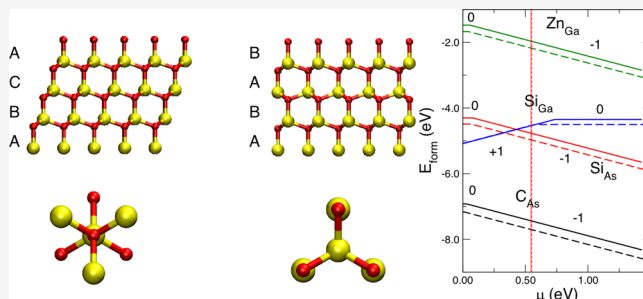Read Online

ACCESS | 📊 Metrics & More | 📖 Article Recommendations | 🆂🅸 Supporting Information

ABSTRACT: The formation energies of n- and p-type dopants in III−V arsenide and phosphide semiconductors (GaAs, GaP, and InP) are calculated within a first-principles total energy approach. Our findings indicate that—for all the considered systems—both the solubility and the *shallowness* of the dopant level depend on the crystal phase of the host material (wurtzite or zincblende) and are the result of a complex equilibrium between local structural distortion and electronic charge reorganization. In particular, in the case of acceptors, we demonstrate that impurities are always more stable in the wurtzite lattice with an associated transition energy smaller with respect to the zincblende case. Roughly speaking, this means that it is easier to p-type dope a wurtzite crystal and the charge carrier concentration at a given temperature and doping dose is larger in the wurtzite as well. As for donors, we show that neutral chalcogen impurities have no clear preference for a specific crystal phase, while charged chalcogen impurities favor substitution in the zincblende structure with a transition energy that is smaller when compared to the wurtzite case (thus, charge carriers are more easily thermally excited to the conduction band in the zincblende phase).

■ INTRODUCTION

Crystal-phase engineering is an emerging field in nanoscience that consists of the design of materials with tailor-made properties by growing *ad hoc* crystal phases. The interest in this field was boosted by the enormous progresses made in recent years in the growth of semiconducting nanowires (NWs)[1,2] and, specifically, by the fact that metastable crystal phases, which in bulk can only be obtained under extreme conditions of temperature and pressure, can be stabilized at room temperature and atmospheric pressure, thanks to a tight control of growth conditions.[3] Many III−V semiconductors, such as arsenides[4−7] and phosphides,[8−11] that in bulk only exhibit the zincblende (ZB) phase, can take the wurtzite (WZ) structure when grown as NWs. Similarly, Si and Ge group-IV semiconductors that in bulk have the 3C cubic-diamond crystal structure can be synthesized in the 2H hexagonal-diamond (*i.e.*, lonsdaleite) polytype.[12−15] The possibility of growing semiconductors in different crystal phases is very appealing, as it might enable novel applications.[16] For instance, ZB GaP has an indirect band gap and thus a limited light emission efficiency, but in WZ GaP NWs, the band gap becomes direct, resulting in a strong photoluminescence.[9] Direct-band gap emission has also been predicted and reported in hexagonal Ge and SiGe alloys,[17,18] materials that have a notoriously poor light emission in the conventional cubic polytype adopted in the bulk. Moreover, in general, different polytypes can present different electronic,[7,19−21] optical,[22−26] and phononic proper-ties.[27−31]

Perhaps, the most ambitious (and exciting) goal of crystal-phase engineering is the design of complex structures by working only (or mostly) with different polytypes of the same material. The conditions that favor the formation of WZ over ZB segments in III−V NWs are well understood[32−34] and can be dynamically tuned during the growth. Therefore, not only isolated *homointerfaces* between the ZB and WZ crystal phase of a same material can be obtained[22,35−37] but also periodic superlattice structures can be obtained. In these crystal-phase superlattices, different polytypes of the same material—rather than different materials, like in conventional superlattices—are arranged periodically, building a metamaterial with its own unique properties, which can be tuned by controlling the number of periods and their thickness.[38−41] These crystal-phase interfaces present some advantages over the most common heterojunctions between two different materials: (i) they have a very small lattice mismatch and (ii) they have no chemical intermixing. As a result, they are atomically flat and virtually defect-free, which makes them ideal candidates to design materials with tailored electronic[38,42,43] and phononic

68　properties.[44,45] Similar effects have also been reported in the
69　less-common crystal-phase core—multishell NWs.[46,47]

70　　The vast majority of applications that can be envisaged in
71　this context rely on impurity doping, which is the primary
72　approach to tune the electrical conductivity of semiconductors.
73　Indeed, the design of electronic devices is based on the
74　juxtaposition of regions with different doping features, for
75　example, in a pn junction, in a bipolar transistor or in a field-
76　effect transistor. Therefore, a detailed understanding of doping
77　in different crystal phases is necessary, both from the viewpoint
78　of the fundamental understanding of the underlying physical
79　mechanisms and for the operation of a multitude of
80　applications. Given a material, is it equally easy to dope it in
81　the ZB and WZ phase? Is the dopant activation energy the
82　same or does it differ in different polytypes? The answers to
83　these questions tell us how the solubility and the charge carrier
84　concentration depend on the crystal phase and have thus far
85　reaching consequences for the design and the optimization of
86　any device.

87　　In this paper, we study by means of first-principles electronic
88　structure calculations of the doping of GaAs, GaP, and InP in
89　the ZB and WZ crystal phase, considering a few common
90　donor and acceptor impurities and an amphoteric impurity (Si
91　in GaAs), whose doping type—donor or acceptor—depends
92　on the sublattice where the substitution takes place. We
93　consider both the neutral and singly charged impurity, thus
94　allowing us to estimate the transition energy, that is, the
95　*shallowness* of the dopant electron state, which determines the
96　concentration of extrinsic charge carriers that are excited in the
97　conduction or valence band for a certain doping dose and at a
98　given temperature, and thus the electrical conductivity. We
99　carry out our calculations in bulk systems, as a reasonable
100　approximation of NWs with diameters of several tens of nm
101　and where quantum confinement effects are negligible, which
102　are commonly used in emergent electronic devices. We
103　observe, nonetheless, that previous results obtained for Si
104　showed that ultrathin NWs (diameters of ∼2 nm) and bulk
105　systems qualitatively exhibit the same behavior regarding the
106　difference between the cubic and hexagonal crystal phase.[43]

■ COMPUTATIONAL METHODS

108　**Electronic Structure Calculations.** We perform density
109　functional theory (DFT) calculations with the VASP code[48]
110　with the local density approximation (LDA) for the exchange—
111　correlation energy functional. We used a plane wave cutoff
112　ranging from 255.2 to 400 eV, depending on the atomic
113　species involved, with the projector augmented-wave meth-
114　od,[49,50] including semicore d electrons for Ga and In. At first,
115　we optimized the lattice parameters of the ZB and WZ
116　primitive cells, sampling the Brillouin zone with a $10 \times 10 \times 10$
117　and $10 \times 10 \times 6$ grid of k-points, respectively. Our results are
118　shown in Table 1. Substitutional impurities at both the group-
119　III and group-V sublattice were studied in $5 \times 5 \times 5$ and 5×5
120　$\times 3$ supercells of the 2- and 4-atom ZB and WZ primitive cells,
121　with a $2 \times 2 \times 2$ grid of k-points. The geometry of the doped
122　supercells was optimized with a quasi-Newton algorithm until
123　all the forces on the atoms were lower than 0.01 eV/Å. This
124　computational setup proved to be accurate enough to give
125　converged values of the formation energy, as shown in previous
126　theoretical studies.[51−54]

127　　We also used density functional perturbation theory
128　(DFPT) to compute the macroscopic dielectric tensor,
129　explicitly accounting for local field effects, which is needed

Table 1. Lattice Parameters, Relative Dielectric Constants, and G_0W_0 Band gaps (LDA Values are Indicated in Parenthesis)

		a (Å)	c (Å)	ε_{xx}	ε_{zz}	bandgap (eV)
GaAs	zincblende	5.601		13.75	13.75	1.66 (0.54)
	wurtzite	3.946	6.510	12.80	13.03	1.46 (0.55)
GaP	zincblende	5.381		10.52	10.52	2.17 (1.39)
	wurtzite	3.790	6.254	10.16	10.60	2.28 (1.32)
InP	zincblende	5.821		11.41	11.41	1.42 (0.62)
	wurtzite	4.107	6.748	10.73	10.96	1.49 (0.68)

for the charge correction scheme described below. We used the 130
optimized lattice vectors and atomic positions obtained at the 131
single-particle DFT level. The computational parameters are 132
the same as for the DFT calculations, but we found that greatly 133
increased k-point meshes are needed to obtain converged 134
results. We used a $36 \times 36 \times 36$ and $36 \times 36 \times 22$ grid for the 135
ZB and WZ polytypes, respectively. The results are 136
summarized in Table 1. 137

On top of the previously optimized primitive cells, we 138
performed *single-shot* G_0W_0 calculations, where quasiparticle 139
energies are calculated from a single GW iteration, that is, using 140
the screened potential (W) as obtained from the DFT (LDA) 141
step. To improve the quality of the results, a large number of 142
real frequency points (200) have been employed for the 143
Hilbert transform of W and self-energy, Σ. Similarly, a very 144
large number of empty bands (∼200) have been included in 145
the calculations to ensure convergence of the results. 146

Handling of Computational Cells with Net Charge. 147
Plane-wave DFT codes, but also localized basis set codes with 148
a Poisson solver based on reciprocal space, assume that the 149
system extends *ad infinitum* with the periodicity set at the 150
input for the computational cell. For charge-neutral systems, 151
this use of periodic boundary conditions (PBCs) is of course 152
well justified in bulk 3D systems, and in lower dimensionalities, 153
it poses no special difficulties, provided that a thick-enough 154
vacuum buffer is added to prevent the interaction between the 155
(spurious) system replicas. 156

The situation is, however, different when addressing systems 157
with isolated net charges, such as the case with an ionized 158
dopant of interest to us here. The long-range Coulomb 159
interaction between the PBC-induced charge replicas will 160
introduce a spurious contribution to the total energy that must 161
be corrected for. Several correction schemes have been 162
proposed[55−58] (see also ref 59 and references therein), often 163
involving the computation of the Madelung energy for some 164
geometric arrangement of point charges in a compensating 165
background.[60,61] In this work, we use a variant of the Makov— 166
Payne scheme[56] that some of us extended to the case of the 167
arbitrary shape of the computational cell and tensor value of 168
the dielectric constant,[62] which is necessary for the hexagonal 169
cells in the WZ case. This type of correction was shown to 170
accelerate convergence in the case of NWs,[63] and thus, it is 171
also expected to do it here. 172

The elements of the dielectric tensor that we have used for 173
our Madelung correction have been obtained from a DFPT 174
calculation as detailed above. We do not consider it necessary 175
to correct these dielectric tensor entries with their 176
experimental counterparts, given that the interaction between 177
the point charge replicas will be screened according to our 178
used theory level, that is, LDA. 179

Formation Energy. The formation energy is the central quantity in defect analysis and it tells us how likely it is to observe a defect in a crystal matrix,[59] either in the case of intrinsic imperfections of the crystal lattice or—the case addressed here—when it comes to an impurity added on purpose to alter in a controlled way the property of a material. The knowledge of the formation energy of a defect delivers some important information concerning the impurity equilibrium concentrations,[64−66] the solubilities,[67,68] or the diffusivities.[69,70] Additionally, by comparing the formation energy of a neutral and singly charged defect, one can obtain the transition energy, a quantity of paramount importance in semiconductor physics that tells us which is the energy needed to thermally excite carriers from the dopant state to the conduction or valence band. The formation energy, as introduced by Zhang and Northrup,[64] is written as follows

$$E_{\text{form}} = E_{\text{tot}}^{\text{D}} - \sum_i n_i \mu_i + q(\mu_{\text{e}} + E_{\text{V}}) \tag{1}$$

where $E_{\text{tot}}^{\text{D}}$ is the total energy of the system including the defect, the sum runs over all the chemical species present, and n_i and μ_i are the number of atoms and chemical potential of species i, respectively. q is the charge state of the defect and μ_{e} is the chemical potential of the electron, which is referred to as E_{V}, the highest occupied eigenvalues of the pristine system. Therefore, μ_{e} varies from 0—at the top of the valence band—to E_{gap}—at the bottom of the conduction band—thus spanning the whole range of doping conditions.

In the case of a compound semiconductor like the ones studied in this work, eq 1 is conveniently reformulated as[65]

$$E_{\text{form}} = E_{\text{D}}^{\text{tot}} - \frac{1}{2}(n_{\text{Ga}} + n_{\text{As}})\mu_{\text{GaAs}}^{\text{bulk}} - \frac{1}{2}(n_{\text{Ga}} - n_{\text{As}})$$
$$(\mu_{\text{Ga}}^{\text{bulk}} - \mu_{\text{As}}^{\text{bulk}} + \Delta\mu) +$$
$$q(\mu_{\text{e}} + E_{\text{V}}) - n_{\text{X}}\mu_{\text{X}} \tag{2}$$

which, for simplicity, is written for the case of GaAs with a generic impurity X. The chemical potentials $\mu_{\text{Ga}}^{\text{bulk}}$, $\mu_{\text{As}}^{\text{bulk}}$, and $\mu_{\text{GaAs}}^{\text{bulk}}$ refer to the bulk compound of Ga, As, and GaAs. We computed $\mu_{\text{Ga}}^{\text{bulk}}$ and $\mu_{\text{As}}^{\text{bulk}}$ as the energy per atom of Ga and As in the orthorhombic and trigonal phase, respectively; for $\mu_{\text{GaAs}}^{\text{bulk}}$, we considered the ZB or WZ crystal phase, depending on the case being addressed. Note that μ_{Ga} and μ_{As} are the chemical potential of Ga and As in GaAs, respectively, and that computing their value is not straightforward. However, one can observe that the chemical potential of bulk GaAs is $\mu_{\text{GaAs}}^{\text{bulk}} = \mu_{\text{Ga}}^{\text{bulk}} + \mu_{\text{As}}^{\text{bulk}} - \Delta H_f$ where ΔH_f is the heat of formation of GaAs. Now, E_{form} is a function of the bulk chemical potential of Ga and As and of the parameter $\Delta\mu$ that accounts for the difference between the chemical potentials of Ga and As in GaAs and in their respective bulk state. The reformulation of E_{form} in eq 2 has the advantage of expressing it in terms of well-defined quantities (the bulk chemical potentials) and of the parameter

$$\Delta\mu = (\mu_{\text{Ga}} - \mu_{\text{As}}) - (\mu_{\text{Ga}}^{\text{bulk}} - \mu_{\text{As}}^{\text{bulk}}) \tag{3}$$

which accounts for the macroscopic stoichiometry conditions of the material. $\Delta\mu$ can vary between $-\Delta H_f$ the limit that corresponds to the As-rich conditions, and ΔH_f for the Ga-rich material, conditions fixed by the inequalities $\mu_{\text{Ga}} \leq \mu_{\text{Ga}}^{\text{bulk}}$

and $\mu_{\text{As}} \leq \mu_{\text{As}}^{\text{bulk}}$. This formalism is also applied to the case of GaP and InP, where we considered the cubic phase for bulk P and the trigonal phase for bulk In to define $\mu_{\text{P}}^{\text{bulk}}$ and $\mu_{\text{In}}^{\text{bulk}}$, respectively.

In the case of the chemical potential of the dopant, μ_{X} (X = Si, C, Zn, S, and Te), we have taken the energy of the isolated atom, assuming that the impurity is incorporated into the crystal from the gas phase. This choice, although sound, is an approximation, because the chemical reservoir where the impurity comes from is not necessarily the one of a monoatomic gas. A different choice would result in a different value of the formation energy (see, *e.g.*, ref 71 for a discussion of the case of H in SiC). Notice, however, that whenever we compare the formation energy of a given impurity in the ZB or WZ crystal phase, μ_{X} cancels out and thus, the conclusions do not depend on its exact value, as already shown in refs 53, 54. The same happens when comparing the formation energy of a dopant in the neutral and singly charged state, which determines the transition energy (neither the transition energy depends on μ_{X}).

■ RESULTS AND DISCUSSION

Stability and Band gap of the Pristine Bulk Systems. Before discussing impurity doping, it is instructive to revise the theory that explains why a given semiconductor adopts one crystal structure or the other, as it will then be important to understand the stability of dopants as well. The simplest way to understand the difference between the ZB and WZ crystal phases is by looking at the stacking sequence along the [111] cubic axis, which is equivalent to the [0001] axis of the WZ. As it is easy to see in Figure 1a,b, in the ZB crystal structure, the
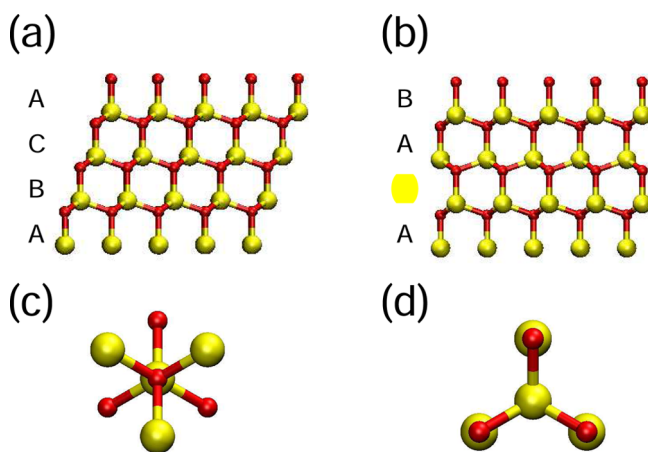

Figure 1. Side view of (a) ZB and (b) WZ lattice structure where the ABCABC *vs* ABABAB stacking along the cubic [111] axis can be appreciated. (c) Staggered and (d) eclipsed dihedral conformation of the ZB and WZ crystal phases.

III−V bilayers are stacked one on top of the other according to an ABCABC stacking motif, while in the WZ one, they follow an ABABAB stacking sequence. When III-arsenides or III-phosphides form, the starting point is always the AB stacking, as the sequence of two bilayers of the same type, for example, AA, is energetically unfavorable. When the next layer grows, it can take the A or C position and thus the ZB or WZ symmetry. In other words, the two polytype structures differ only in the eclipsed (WZ) or staggered (ZB) dihedral conformation that in turn affects the 1,4 atomic interactions (see in Figure 1c,d).

Under such conditions, the preference for one of the two crystal phases is the result of a competition between covalent and ionic contributions.[72,73] For compounds following the octet rule, $A^N B^{8-N}$, the WZ structure is favored when the ionic component is strong. The limiting case is constituted by group-IV semiconductors, that is, Si, Ge, and diamond, where the bond is fully covalent and that accordingly adopt the cubic structure. Then, in III−V semiconductors, the larger the ionic contribution is, the less the ZB phase will be favored over the WZ one, until the latter becomes the ground state as in GaN.

Our results agree well with this picture, as we found that the preference for the ZB structure according to our calculations is 21.9 meV for GaAs, 17.4 meV for GaP, and 10.6 meV for InP per unit formula (f.u.), which follows a prediction based on the electronegativity differences between the anion and cation according to the Pauling scale, a crude measure of the ionicity of the bond: 0.37 for GaAs, 0.38 for GaP, and 0.41 in InP. Therefore, the larger the electronegativity difference is, the more ionic is the bond and the less favored is the ZB crystal phase. A more refined definition of the ionicity of a bond is the so-called atomic asymmetry parameter (AAS) between a pair of atoms,[74,75] which is known to work well in crystals of the $A^N B^{8-N}$ type. The AAS values for GaAs, GaP, and InP are 0.316, 0.371, and 0.506, respectively, which are also in good agreement with the abovementioned energy preferences. Other criteria to estimate the ionic character of the chemical bond are of course possible; see, for example, the ionicity scale based on the centers of maximally localized Wannier functions of Abu-Farsakh and Qteish.[76]

One of the reasons of interest in crystal-phase engineering is the tunability of the electronic properties. Therefore, another issue that we addressed and briefly discuss before moving to the case of extrinsic doping is the dependence of the electronic band gap on the crystal phase. As it is well known, DFT in its local and semilocal approximation of the exchange−correlation energy severely underestimates the band gap. Therefore, we have performed quasiparticle $G_0 W_0$ calculations that allow bypassing this limitation. The results are reported in Table 1.

The electronic properties of bulk ZB GaAs have been investigated from first principles since decades in view of the microelectronic-oriented applications of the material[77−80] and theoretically assessing the band gap of GaAs main polymorphs remains controversial, as a definitive conclusion is still missing (see ref 16 for a detailed discussion). Furthermore, although on one side, there is a large availability of experimental data about ZB GaAs (see, *e.g.*, refs 81, 82), the scarcity of experimental data about WZ GaAs samples, mostly derived by NW structures, makes the comparison with experimental data for this polymorph a quite cumbersome task because of the expected overestimation of the gap due to quantum confine-ment effects. Indeed, there are experimental reports for the band gap of WZ-GaAs NWs to be either larger or smaller than the one of ZB-GaAs NWs by few tens of meV.[16]

A good description and comparison between DFT- and *GW*-calculated electronic properties of the two polymorphs of GaAs have been provided by Zanolli *et al.*:[83] their LDA-calculated value for WZ GaAs is 50 meV larger than the ZB-calculated one, in good agreement with our findings (the absolute values differ because Zanolli *et al.* used a different, custom-made pseudopotential[84]) and with those of Yeh *et al.*[78] On the other hand, the *GW* values they obtained are 1.133 eV (ZB) and 1.351 eV (WZ), while at the quasiparticle level, we found the

band gap of ZB GaAs to be larger than that of WZ GaAs (see Table 1).

A similar problem can be encountered in the case of InP and GaP. Because the WZ bulk phase of these compounds is not stable under normal conditions, all the experimental data concerning its band gap are derived from indirect measure-ments on NWs (in which instead the WZ phase can be stabilized). The theoretical and experimental literature addressing this issue is less extensive when compared to that on GaAs. The band gap of WZ InP has been experimentally reported to be slightly larger than that of ZB InP (see for instance refs 85, 86), in agreement with our results (see Table 1) and other theoretical calculations.[87] On the other hand, a limited number of experiments have been performed to investigate the band gap of WZ GaP,[9,26] which is expected to be around 2.19 eV. This value is not far from what we calculated (2.28 eV) and other *ab initio* quasiparticle calculations.[88]

Impurity Doping: Stability and Transition Energies.
General Considerations. Band theory of semiconductors relies on a perfect duality between n- and p-type doping, where electrons and holes are thermally excited from the impurity state to the conduction and valence band. Microscopically, however, this duality breaks down because chemical bonds are formed by electrons only. Therefore, the case of donors, where the four bonds of a tetrahedral semiconductor can be satisfied and there is an additional, loosely bound electron, is different from the case of acceptors, where the substitutional impurity only has three electrons to form bonds.

In the ZB phase, all atoms occupy the center of a perfect tetrahedron with all four first neighbor distances equal (T_d symmetry). This local symmetry is maintained in the case of doping with deformations consisting of the sole uniform contraction or expansion of the bond length. In the WZ phase, each atom has three equidistant first neighbors, while the fourth neighbor, along the *c* direction, is usually more far apart (C_{3v} symmetry). The WZ structure has thus more structural freedom to adjust to perturbations induced by impurities because the variations in the bonding can be tuned by the fact that there are two different types of bonds. Therefore, when an acceptor is introduced in the lattice, it will try to form three bonds, something that is favored in the WZ structure where three of the bonds can become stronger and one weaker, the final outcome being the stabilization of the lattice. This does not happen in the ZB lattice. Thus, introducing electron deficiency in the pristine III−V solids provides a bias for the WZ structure.[53]

Another way of tuning the WZ−ZB stability is by altering the ionic component of the bonding. In III−V solids, the bond is always partly ionic and one partner is electron-rich, whereas the other is electron-poor. Adding electrons or holes has different effects: adding electrons increases the electronic asymmetry and thus the ionic contribution, whereas adding holes decreases the electronic asymmetry and thus the ionic contribution. According to the discussion in the previous section, an increased ionicity favors the WZ lattice, while more covalent bonds favor the ZB. Therefore, adding (removing) electrons is expected to stabilize the WZ (ZB) crystal phase.

Acceptors. We now move to the discussion of the main results of our study and start with impurities that provide p-type doping. We computed the formation energies of five different systems doped with an acceptor: C_{As}@GaAs, Si_{As}@GaAs, Zn_{Ga}@GaAs, Zn_{Ga}@GaP, and Zn_{In}@InP, where the

notation C_{As}@GaAs stands for a C atom substituting an As atom in a GaAs lattice (and likewise for the other cases). In all the cases, we considered the neutral charge state and the −1 charge state, which is expected to be the more stable charge state when the Fermi level lies above the dopant level. These are all textbook cases of acceptors, where an atom of the lattice is substituted by an impurity from the group of the periodic table immediately to its left. Impurities from group-IV can, in principle, be both donors and acceptors, depending on the sublattice chosen for the substitution.[89] This is the case of Si@GaAs, which acts as an acceptor when it substitutes an As atom and as a donor when it substitutes a Ga atom. C could behave similarly, but substitution at the As sublattice is much more stable than substitution at the Ga sublattice (we found a difference of 0.27 and 0.37 eV in ZB and WZ GaAs, respectively), so the latter in practice never occurs. We recall that we carried out our calculations in bulk systems, as an approximation of realistic, large-diameter NWs. For a study of extrinsic defects in GaAs NWs, the interested reader can see, for example, the studies of Galicka et al.[90] and Diao et al.;[91] intrinsic defects in GaAs and their relation with polytypism have been explored by Du et al.[92]

The results of the formation energy as a function of the chemical potential of the electron for GaAs are shown in Figure 2. As it can be seen, all the three acceptors have some

Figure 2. Formation energies as a function of the chemical potential of the electron of Si, C, and Zn in ZB (continuous line) and WZ (dashed line) GaAs. The side panels show zoomed-in views of Si_{As} (top) and Si_{Ga} (bottom).

features in common: (i) the neutral impurity is always more stable in the WZ lattice, for all values of μ_e (see dashed lines in Figure 2); (ii) the increased stability is similar in all the cases; and (iii) the transition energy is (slightly) smaller in the WZ and the impurity state is *shallower* (see the zoomed view for Si_{As}@GaAs). Simply put, it is easier to p-type dope GaAs in the WZ phase and these dopants will be easier to activate.

Following the arguments given above, we now attempt to rationalize the observed behavior. A very important factor to consider in understanding the role of the impurity is the mismatch between the impurity and the host lattice. The four Ga−As bond lengths in pristine WZ GaAs are 2.422 (×3) and 2.433 Å. Let us consider the case of Si_{As}@GaAs (the full list of

bond lengths is given in the Supporting Information). The Si−As bond lengths around the impurity are 2.348 (×3) and 2.353 Å, that is, they are all shorter because Si is smaller than As. The four distances associated with the four nearest neighbor Ga atoms are 2.440−2.430 (×3) and 2.348−2.353 Å. This means that the structural perturbation of the impurity is almost limited to the second coordination sphere of the impurity. However, more important to notice is the fact that the three bonds for every nearest neighbor of the impurity connecting with the rest of the GaAs lattice are longer than in the pristine. In other words, the stabilizing effect due to the four bonds of the Si impurity is at least partially compensated by the destabilization of the 12 Ga−As bonds of the second coordination sphere. Of course, this effect occurs even more intensely for the case of C_{As}@GaAs. A different situation occurs for Zn_{Ga}@GaAs. In that case, the Zn−As distances are 2.395 (×3) and 2.397 Å, which are shorter than the initial ones but not as much as for Si. However, now, the distances connecting the four nearest neighbors with the rest of the GaAs lattice are all around 2.390−2.400 Å, that is, they are all shorter than the initial ones. Clearly, the better match between the impurity and the host lattice allows a weaker but better balanced distortion of the lattice, which avoids the above-mentioned destabilization of 12 bonds and transforms it into stabilization.

For all neutral acceptor impurities studied (Table 2), we find that whatever the mismatch is, the WZ structure is clearly
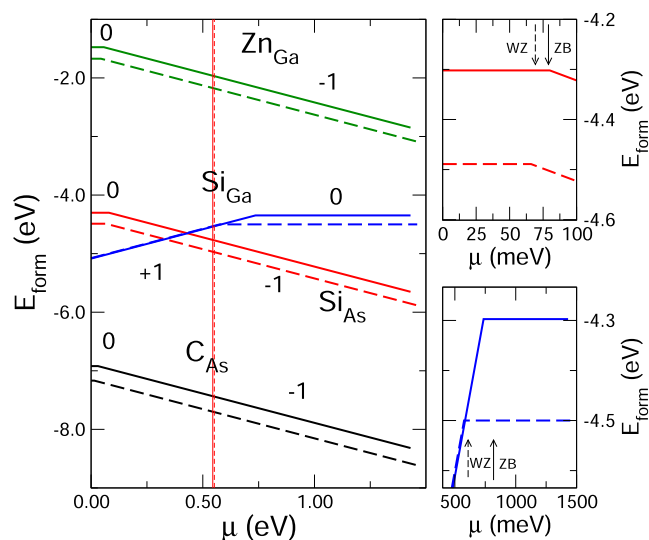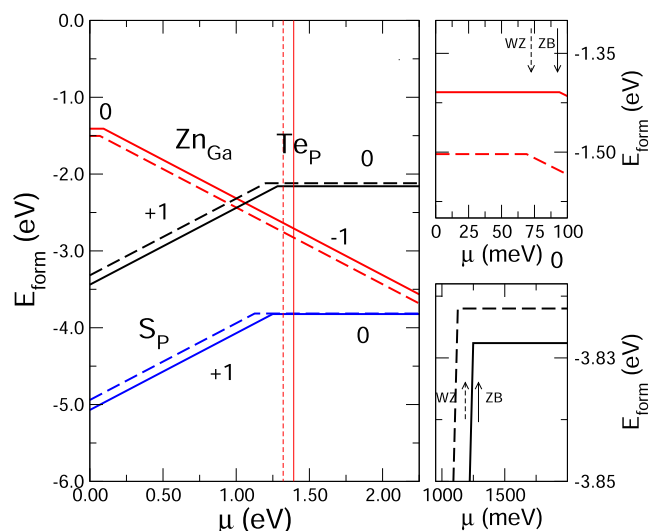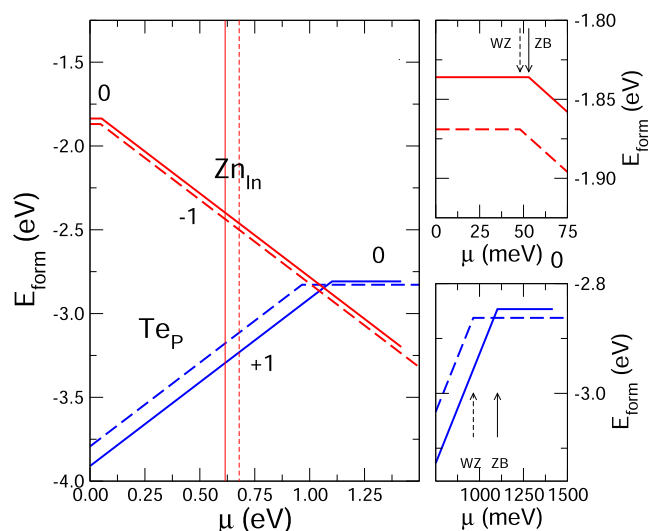
Table 2. Difference in the Neutral and Charged Impurity Formation Energy, ΔE_{form}, between the ZB and WZ Structures (a Positive Value Indicates That the WZ Is More Stable) for the Series of Acceptor Impurities Studied[a]

	GaAs			GaP	InP
	Si_{As}	C_{As}	Zn_{Ga}	Zn_P	Zn_P
ΔE_{form}^{0}	187	248	197	94	33
ΔE_{form}^{-1}	201	265	210	119	39
$\Delta E(0/-)$	14	17	13	25	6

[a]All energies are given in meV/f.u. We also report the difference in transition energies, $\Delta E(0/-)$, between the ZB and WZ structures (a positive value indicates that the impurity state in WZ is shallower).

preferred. This is the consequence of two features, both already anticipated in the discussion in the previous section: (i) acceptor impurities generate electron deficiency in the already electron-deficient sites of the lattice and (ii) as far as the impurity is smaller or similar in size to the original host atom, the induced structural perturbation is more easily accommodated within the WZ lattice because of the larger structural freedom degrees allowing a 3 + 1-type coordination. As shown in Table 2, this preference is even increased for charged impurities. Thus, the transition energies for acceptor impurities are always smaller (i.e., the impurity level is closer to the valence band, $\Delta E(0/-)$, in Table 2) in the WZ structure. If we consider impurities in the GaAs lattice, it is clear that the increase in the preference when the impurity is charged is an almost constant value (the only exception is singly charged Si that does not favor any crystal phase). By analyzing the Bader charges before and after the charging, we could conclude that there is barely any change at the impurity and four nearest neighbor sites, thus suggesting that the hole resulting from the acceptor impurity must be very delocalized in the lattice. Because adding an electron increases the charge asymmetry,

the WZ should be further stabilized over the ZB because of the charging, although the effect is only modest for acceptor impurities. Consequently, our calculations suggest that smaller transition energies will be associated with larger stabilizations of the WZ structure for the neutral impurity.

All these considerations are straightforwardly extended to the case of Zn_{Ga}@GaP and Zn_{In}@InP, whose formation energies are shown in Figures 3 and 4, and thus confirm the generality of the trends discussed.

Figure 3. Formation energies as a function of the chemical potential of the electron of Te, S, and Zn in ZB (continuous line) and WZ (dashed line) GaP. The side panels show zoomed-in views of Zn_{Ga} (top) and Te_P (bottom).

Figure 4. Formation energies as a function of the chemical potential of the electron of Te and Zn in ZB (continuous line) and WZ (dashed line) InP. The side panels show zoomed-in views of Zn_{In} (top) and Te_P (bottom).

Donors. We considered four different systems doped with a donor: Si_{Ga}@GaAs, S_P@GaP, Te_P@GaP, and Te_P@InP. In all these cases, an atom of the lattice is substituted by an impurity from the group of the periodic table immediately to its right. We studied each impurity in the neutral and +1 charge state, which is expected to be the more stable charge state when the Fermi level lies below the dopant level. As mentioned above, Si is an amphoteric dopant, so although Si_{As}@GaAs is an acceptor, here, we study Si_{Ga}@GaAs that acts as a donor.

The results of the formation energy as a function of the chemical potential of the electron for the three compounds investigated are shown in Figures 2−4. Also, in this case, it is possible to highlight some common features: (i) neutral chalcogen impurities, S and Te, show no clear preference for the ZB or WZ crystal phase; (ii) charged chalcogen impurities favor substitution in the ZB structure; and (iii) the transition energy is smaller in the ZB, that is, the impurity state is *shallower* (see the zoomed-in view of Si_{Ga}@GaAs, Te_P@GaP, and Te_P@InP in the side panels). Therefore, at variance with the case of acceptors, donor impurities are more easily activated in the ZB crystal phase, while their solubility is larger in ZB structures when the impurities are in the +1 charge state. We note that occasionally, the transition energy falls within the conduction band, this being a known shortcoming of using LDA to account for the exchange–correlation energy and thus of the underestimation of the band gap. We have indeed computed much more accurate band gaps from G_0W_0 calculations, but treating the doped supercells at the same level of the theory is beyond the current computational capabilities and, obviously, single-particle and many-body results cannot be mixed together. Therefore, the conclusions directly related to transition energies obtained from DFT−LDA calculations can only be taken to be semiquantitative,[59] and approaches that suggest to ignore the calculated band edges and reference charge transition levels to marker levels[93] or to the average electrostatic potential[94−96] have been proposed. We recall once again, however, that our main goal is understanding the difference between doping with a certain impurity the ZB and WZ crystal phase of a given semiconductor and not to quantitatively estimate the transition energies. Hence, we argue that all the conclusions based on such comparisons are robust and the physical insight they provide is reliable.

The donors that we studied belong to two different categories. When P is substituted by S or Te neutral impurities, a structural perturbation different from that discussed above takes place. Both atoms are strongly electronegative and although they act as donors toward the lattice by generating an extra electron, they also gain electron density. For instance, the calculated Bader charges for S_P@GaP and Te_P@GaP are 6.85 and 6.38 e^-, respectively, in the WZ structure and 6.83 and 6.42 e^- in the ZB structure (for comparison, the Bader charge of P in the pristine GaP lattice amounts to 5.70 e^- in the ZB and 5.72 e^- in the WZ; remember that because of the inclusion of 3d electrons in the valence of the Ga atom, the total charge for each Ga−P pair is 18 e^-). In fact, this electronic gain mostly originates from the polarization of the bonds between the very electronegative chalcogen atom and the weakly electronegative Ga atom. The important structural observation is that in contrast with acceptors, the bonds between chalcogen and the four nearest neighbors become clearly longer than in the pristine crystal. For instance, the Ga−P bonds in WZ GaP are 2.327 (×3) and 2.338 Å. The X−Ga (X = S and Te) bond lengths around the impurity in X_P@GaP are as long as 2.407 (×3) and 2.413 Å for X = S and 2.610 (×3) and 2.617 Å for X = Te. The anionic chalcogen atoms, with their high electron density, strongly push the four nearest neighbor atoms, compressing the lattice around the second coordination sphere of the impurity. Under such circum-

561 stances, the additional structural degree of freedom of the WZ
562 structure becomes considerably less effective and the very
563 isotropic nature of the ZB structure becomes comparable or
564 even slightly preferred. Only for the more expanded lattice of
565 InP, the WZ structure is again slightly favored (see Table 3).

Table 3. Difference in the Neutral and Charged Impurity Formation Energy, ΔE_{form}, between the ZB and WZ Structures (a Positive Value Indicates That the WZ Is More Stable) for the Series of Donor Impurities Studied[a]

	GaAs	GaP		InP
	Si_{Ga}	S_P	Te_P	Te_P
$\Delta E_{\text{form}}{}^{0}$	152	−7	−39	20
$\Delta E_{\text{form}}{}^{+1}$	−8	−130	−122	−117
$\Delta E(+/0)$	160	123	83	137

[a]All energies are given in meV/f.u. We also report the difference in transition energies, $\Delta E(+/0)$, between the ZB and WZ structures (a positive value indicates that the impurity state in ZB is shallower).

566 In contrast, because of the structural mismatch, Si_{Ga}@GaAs
567 behaves in the same way described above for the case where Si
568 was acting as an acceptor; the only difference is that the short
569 distances with the four nearest neighbors are now a bit longer
570 (i.e., 2.372 (×3) and 2.382 Å for Si_{Ga} compared with 2.348
571 (×3) and 2.353 Å for Si_{As} in GaAs WZ). Thus, according to
572 our calculations, Si in GaAs has a preference for WZ
573 irrespective of acting as a donor or an acceptor. In fact, the
574 calculated energy differences are comparable (187 meV/f.u. for
575 Si_{As} and 152 meV/f.u. for Si_{Ga}). This result emphasizes the key
576 role of the mismatch in enforcing the WZ−ZB preference.

577 Note that among the different impurities studied, charging
578 the impurity always favors the ZB structure even when the
579 impurity is smaller than the host atom replaced (Table 3). This
580 contribution is relatively large and finally determines the
581 preference of all donor impurities studied for the ZB structure.
582 We believe the origin of this result is that, as noted above,
583 removing the electron provided by the neutral impurity
584 decreases the ionicity of the lattice and consequently, the ZB
585 structure is favored. According to our calculations, for donors
586 compressing the lattice around the impurity, the shallowness
587 will increase with the size of the impurity and/or decreasing
588 the cell constants of the pristine lattice.

589 As a final remark, we observe that our computed transition
590 energies, indicating that donor states are shallower in the ZB
591 crystal phase, agree well with the predictions of the hydrogenic
592 model of substitutional impurities within effective mass theory
593 (EMT). Within this simple model, the substitutional impurity
594 form four bonds with the nearest neighbors, with negligible
595 relaxation effects and charge transfer, leaving one unpaired
596 electron whose energy is approximately given by

$$E_n \sim -\text{Ry}\frac{m^*}{\varepsilon^2 n^2} \tag{4}$$

597

598 where m^* is the effective mass in units of the electron mass, n
599 is the main quantum number, ε is the (relative) static dielectric
600 constant, and Ry is the Rydberg constant. This is the quantum
601 mechanical solution of the hydrogen atom except for the fact
602 that it contains parameters of the bulk host crystal, such as m^*
603 and ε. E_n is the energy of the unpaired electron relative to the
604 conduction band minimum, so large values of ε and small
605 values of m^* both contribute to make the impurity shallower,

606 that is, E_n small. If we look at the computed values of the static
607 dielectric constant collected in Table 1, we see that for GaAs,
608 GaP, and InP, when going from the ZB to the WZ, it decreases
609 (with a reduction, i.e., slightly more pronounced for the zz
610 component of the tensor). As for the electron effective mass, it
611 has been shown experimentally that it is heavier in the WZ
612 than in the ZB,[36,37,97,98] a trend corroborated by our
613 calculations. Therefore, both these effects tend to make the
614 impurity state deeper in the WZ, in agreement with the
615 computed transition energies. EMT also provides an estimate
616 for the effective Bohr radius of the ground state, which is

$$a_B \sim (\varepsilon/m^*)a_0 \tag{5}$$

617

618 where $a_0 \sim 0.577$ Å is the Bohr radius of the isolated hydrogen
619 atom. The effective Bohr radius gives a useful indication of the
620 distance over which the dopant wavefunction extends. This
621 value ranges from 0.5 to 11 nm, indicating that the
622 wavefunction can be considerably delocalized and that the
623 donor electron loosely binds to the dopant atom. This
624 observation agrees with the computed Bader charges of the
625 donors that barely change when the system goes from neutral
626 to charged, that is, the additional charge effectively spreads all
627 over the atoms of the supercell.

CONCLUSIONS

629 We have presented first-principles density functional calcu-
630 lations of impurity doping in GaAs, GaP, and InP, comparing
631 their stability and transition energies when dopants are
632 introduced in the ZB or in the WZ. The cubic ZB crystal
633 structure is the common crystal phase of bulk arsenides and
634 phosphides, but doping of the WZ is becoming increasingly
635 important because this crystal phase can be stabilized even at
636 room temperature and atmospheric pressure when these
637 semiconductors are grown as NWs. Our results highlight a
638 general trend where acceptors favor substitution in WZ
639 crystals, where they have a shallower electronic state, allowing
640 an easier excitation of charge carriers for band transport. The
641 situation is reversed for donors, which feature a shallower
642 impurity state and higher solubilities in the ZB. These
643 observations are rationalized in terms of the local distortion
644 and electronic charge reorganization upon doping. In
645 particular, we show that (i) the reduced symmetry of the
646 WZ is better suited to accommodate the local relaxation of
647 acceptors, which favors a three-fold coordination and (ii) ionic
648 bonds favor the WZ lattice, while more covalent bonds favor
649 the ZB and the ionic character of the bond can be increased
650 (decreased) by adding electrons (holes). These results are
651 important for the design and optimization of electronic devices
652 based on semiconducting NWs in the growing field of crystal-
653 phase engineering.

ASSOCIATED CONTENT

Supporting Information

The Supporting Information is available free of charge at
https://pubs.acs.org/doi/10.1021/acs.jpcc.0c09391.

First-neighbor distances of the pristine crystal, of the
impurity, and of the four first neighbors (PDF)

AUTHOR INFORMATION

Corresponding Authors

Enric Canadell − *Institut de Ciència de Materials de
Barcelona, ICMAB-CSIC, 08193 Bellaterra, Spain;*

orcid.org/0000-0002-4663-5226; Email: canadell@icmab.es

Riccardo Rurali − *Institut de Ciència de Materials de Barcelona, ICMAB-CSIC, 08193 Bellaterra, Spain;* orcid.org/0000-0002-4086-4191; Email: rrurali@icmab.es

Authors

Giacomo Giorgi − *Department of Civil and Environmental Engineering, University of Perugia (DICA), 06125 Perugia, Italy; CNR-SCITEC, 06123 Perugia, Italy;* orcid.org/0000-0003-4892-7908

Michele Amato − *Université Paris-Saclay, CNRS, Laboratoire de Physique des Solides, 91405 Orsay, France;* orcid.org/0000-0002-3690-3194

Stefano Ossicini − *"Centro S3", CNR-Istituto di Nanoscienze, 41125 Modena, Italy; Dipartimento di Scienze e Metodi dell'Ingegneria, Centro Interdipartimentale En&Tech, Universitá di Modena e Reggio Emilia, I-42100 Reggio Emilia, Italy*

Xavier Cartoixà − *Departament d'Enginyeria Electrònica, Universitat Autònoma de Barcelona, 08193 Bellaterra, Barcelona, Spain;* orcid.org/0000-0003-1905-5979

Complete contact information is available at:
https://pubs.acs.org/10.1021/acs.jpcc.0c09391

Author Contributions

∇G.G. and M.A. contributed equally to this work.

Notes

The authors declare no competing financial interest.

■ REFERENCES

(1) Wang, N.; Cai, Y.; Zhang, R. Q. Growth of nanowires. *Mater. Sci. Eng., R* **2008**, *60*, 1−51.

(2) Schmidt, V.; Wittemann, J. V.; Senz, S.; Gösele, U. Silicon Nanowires: A Review on Aspects of their Growth and their Electrical Properties. *Adv. Mater.* **2009**, *21*, 2681−2702.

(3) Caroff, P.; Bolinsson, J.; Johansson, J. Crystal Phases in III−V Nanowires: From Random Toward Engineered Polytypism. *IEEE J. Sel. Top. Quantum Electron.* **2011**, *17*, 829−846.

(4) Koguchi, M.; Kakibayashi, H.; Yazawa, M.; Hiruma, K.; Katsuyama, T. Crystal Structure Change of GaAs and InAs Whiskers from Zinc-Blende to Wurtzite Type. *Jpn. J. Appl. Phys., Part 1* **1992**, *31*, 2061.

(5) Persson, A. I.; Larsson, M. W.; Stenström, S.; Ohlsson, B. J.; Samuelson, L.; Wallenberg, L. R. Solid-phase diffusion mechanism for GaAs nanowire growth. *Nat. Mater.* **2004**, *3*, 677−681.

(6) Harmand, J. C.; Patriarche, G.; Péré-Laperne, N.; Mérat-Combes, M.-N.; Travers, L.; Glas, F. Analysis of vapor-liquid-solid mechanism in Au-assisted GaAs nanowire growth. *Appl. Phys. Lett.* **2005**, *87*, 203101.

(7) Funk, S.; Li, A.; Ercolani, D.; Gemmi, M.; Sorba, L.; Zardo, I. Crystal Phase Induced Bandgap Modifications in AlAs Nanowires Probed by Resonant Raman Spectroscopy. *ACS Nano* **2013**, *7*, 1400−1407.

(8) Mohan, P.; Motohisa, J.; Fukui, T. Controlled growth of highly uniform, axial/radial direction-defined, individually addressable InP nanowire arrays. *Nanotechnology* **2005**, *16*, 2903.

(9) Assali, S.; Zardo, I.; Plissard, S.; Kriegner, D.; Verheijen, M. A.; Bauer, G.; Meijerink, A.; Belabbes, A.; Bechstedt, F.; Haverkort, J. E. M.; Bakkers, E. P. A. M. Direct Band Gap Wurtzite Gallium Phosphide Nanowires. *Nano Lett.* **2013**, *13*, 1559−1563.

(10) Vu, T. T. T.; Zehender, T.; Verheijen, M. A.; Plissard, S. R.; Immink, G. W. G.; Haverkort, J. E. M.; Bakkers, E. P. A. M. High optical quality single crystal phase wurtzite and zincblende InP nanowires. *Nanotechnology* **2013**, *24*, 115705.

(11) Lehmann, S.; Wallentin, J.; Mårtensson, E. K.; Ek, M.; Deppert, K.; Dick, K. A.; Borgström, M. T. Simultaneous Growth of Pure Wurtzite and Zinc Blende Nanowires. *Nano Lett.* **2019**, *19*, 2723−2730.

(12) Vincent, L.; Patriarche, G.; Hallais, G.; Renard, C.; Gardès, C.; Troadec, D.; Bouchier, D. Novel Heterostructured Ge Nanowires Based on Polytype Transformation. *Nano Lett.* **2014**, *14*, 4828−4836.

(13) Hauge, H. I. T.; Verheijen, M. A.; Conesa-Boj, S.; Etzelstorfer, T.; Watzinger, M.; Kriegner, D.; Zardo, I.; Fasolato, C.; Capitani, F.; Postorino, P.; Kölling, S.; Li, A.; Assali, S.; Stangl, J.; Bakkers, E. P. A. M. Hexagonal Silicon Realized. *Nano Lett.* **2015**, *15*, 5855−5860.

(14) Hauge, H. I. T.; Conesa-Boj, S.; Verheijen, M. A.; Koelling, S.; Bakkers, E. P. A. M. Single-Crystalline Hexagonal Silicon-Germanium. *Nano Lett.* **2017**, *17*, 85−90.

(15) Vincent, L.; Djomani, D.; Fakfakh, M.; Renard, C.; Belier, B.; Bouchier, D.; Patriarche, G. Shear-driven phase transformation in silicon nanowires. *Nanotechnology* **2018**, *29*, 125601.

(16) Tizei, L. H. G.; Amato, M. Electronic structure and optical properties of semiconductor nanowires polytypes. *Eur. Phys. J. B* **2020**, *93*, 16.

(17) Cartoixà, X.; Palummo, M.; Hauge, H. I. T.; Bakkers, E. P. A. M.; Rurali, R. Optical Emission in Hexagonal SiGe Nanowires. *Nano Lett.* **2017**, *17*, 4753−4758.

(18) Fadaly, E. M. T.; Dijkstra, A.; Suckert, J. R.; Ziss, D.; van Tilburg, M. A. J.; Mao, C.; Ren, Y.; van Lange, V. T.; Korzun, K.; Kölling, S.; et al. Direct-bandgap emission from hexagonal Ge and SiGe alloys. *Nature* **2020**, *580*, 205−209.

(19) Zardo, I.; Yazji, S.; Hörmann, N.; Hertenberger, S.; Funk, S.; Mangialardo, S.; Morkötter, S.; Koblmüller, G.; Postorino, P.; Abstreiter, G. E1(A) Electronic Band Gap in Wurtzite InAs Nanowires Studied by Resonant Raman Scattering. *Nano Lett.* **2013**, *13*, 3011−3016.

(20) De Luca, M.; Polimeni, A. Electronic properties of wurtzite-phase InP nanowires determined by optical and magneto-optical spectroscopy. *Appl. Phys. Rev.* **2017**, *4*, 041102.

(21) Senichev, A.; Corfdir, P.; Brandt, O.; Ramsteiner, M.; Breuer, S.; Schilling, J.; Geelhaar, L.; Werner, P. Electronic properties of wurtzite GaAs: A correlated structural, optical, and theoretical analysis of the same polytypic GaAs nanowire. *Nano Res.* **2018**, *11*, 4708−4721.

(22) Spirkoska, D.; Arbiol, J.; Gustafsson, A.; Conesa-Boj, S.; Glas, F.; Zardo, I.; Heigoldt, M.; Gass, M. H.; Bleloch, A. L.; Estrade, S.; et al. Structural and optical properties of high quality zinc-blende/wurtzite GaAs nanowire heterostructures. *Phys. Rev. B: Condens. Matter Mater. Phys.* **2009**, *80*, 245325.

(23) Heiss, M.; Conesa-Boj, S.; Ren, J.; Tseng, H.-H.; Gali, A.; Rudolph, A.; Uccelli, E.; Peiró, F.; Morante, J. R.; Schuh, D.; Reiger, E.; Kaxiras, E.; Arbiol, J.; Fontcuberta i Morral, A. Direct correlation of crystal structure and optical properties in wurtzite/zinc-blende GaAs nanowire heterostructures. *Phys. Rev. B: Condens. Matter Mater. Phys.* **2011**, *83*, 045303.

(24) De Luca, M.; Zilli, A.; Fonseka, H. A.; Mokkapati, S.; Miriametro, A.; Tan, H. H.; Smith, L. M.; Jagadish, C.; Capizzi, M.; Polimeni, A. Polarized Light Absorption in Wurtzite InP Nanowire Ensembles. *Nano Lett.* **2015**, *15*, 998−1005.

(25) Zilli, A.; De Luca, M.; Tedeschi, D.; Fonseka, H. A.; Miriametro, A.; Tan, H. H.; Jagadish, C.; Capizzi, M.; Polimeni, A. Temperature Dependence of Interband Transitions in Wurtzite InP Nanowires. *ACS Nano* **2015**, *9*, 4277−4287.

(26) Assali, S.; Greil, J.; Zardo, I.; Belabbes, A.; de Moor, M. W. A.; Koelling, S.; Koenraad, P. M.; Bechstedt, F.; Bakkers, E. P. A. M.; Haverkort, J. E. M. Optical study of the band structure of wurtzite GaP nanowires. *J. Appl. Phys.* **2016**, *120*, 044304.

(27) Zardo, I.; Conesa-Boj, S.; Peiro, F.; Morante, J. R.; Arbiol, J.; Uccelli, E.; Abstreiter, G.; Fontcuberta i Morral, A. Raman spectroscopy of wurtzite and zinc-blende GaAs nanowires: Polarization dependence, selection rules, and strain effects. *Phys. Rev. B: Condens. Matter Mater. Phys.* **2009**, *80*, 245324.

(28) Raya-Moreno, M.; Aramberri, H.; Seijas-Bellido, J. A.; Cartoixà, X.; Rurali, R. Thermal conductivity of hexagonal Si and hexagonal Si nanowires from first-principles. *Appl. Phys. Lett.* **2017**, *111*, 032107.

(29) Raya-Moreno, M.; Rurali, R.; Cartoixà, X. Thermal conductivity for III-V and II-VI semiconductor wurtzite and zinc-blende polytypes: The role of anharmonicity and phase space. *Phys. Rev. Mater.* **2019**, *3*, 084607.

(30) Fasolato, C.; De Luca, M.; Djomani, D.; Vincent, L.; Renard, C.; Di Iorio, G.; Paillard, V.; Amato, M.; Rurali, R.; Zardo, I. Crystalline, Phononic, and Electronic Properties of Heterostructured Polytypic Ge Nanowires by Raman Spectroscopy. *Nano Lett.* **2018**, *18*, 7075−7084.

(31) de Matteis, D.; De Luca, M.; Fadaly, E. M. T.; Verheijen, M. A.; López-Suárez, M.; Rurali, R.; Bakkers, E. P. A. M.; Zardo, I. Probing Lattice Dynamics and Electronic Resonances in Hexagonal Ge abd Si_xGe_{1-x} Alloys in Nanowires by Raman Spectroscopy. *ACS Nano* **2020**, *14*, 6845−6856.

(32) Glas, F.; Harmand, J.-C.; Patriarche, G. Why Does Wurtzite Form in Nanowires of III-V Zinc Blende Semiconductors? *Phys. Rev. Lett.* **2007**, *99*, 146101.

(33) Dubrovskii, V. G.; Sibirev, N. V.; Harmand, J. C.; Glas, F. Growth kinetics and crystal structure of semiconductor nanowires. *Phys. Rev. B: Condens. Matter Mater. Phys.* **2008**, *78*, 235301.

(34) Dubrovskii, V. G.; Sibirev, N. V. Growth thermodynamics of nanowires and its application to polytypism of zinc blende III-V nanowires. *Phys. Rev. B: Condens. Matter Mater. Phys.* **2008**, *77*, 035414.

(35) Zheng, H.; Wang, J.; Huang, J. Y.; Wang, J.; Zhang, Z.; Mao, S. X. Dynamic Process of Phase Transition from Wurtzite to Zinc Blende Structure in InAs Nanowires. *Nano Lett.* **2013**, *13*, 6023−6027.

(36) Corfdir, P.; Van Hattem, B.; Uccelli, E.; Conesa-Boj, S.; Lefebvre, P.; Fontcuberta i Morral, A.; Phillips, R. T. Three-Dimensional Magneto-Photoluminescence as a Probe of the Electronic Properties of Crystal-Phase Quantum Disks in GaAs Nanowires. *Nano Lett.* **2013**, *13*, 5303−5310.

(37) Tedeschi, D.; Fonseka, H. A.; Blundo, E.; del Águila, A. G.; Guo, Y.; Tan, H. H.; Christianen, P. C. M.; Jagadish, C.; Polimeni, A.; De Luca, M. Hole and Electron Effective Masses in Single InP Nanowires with a Wurtzite-Zincblende Homojunction. *ACS Nano* **2020**, *14*, 11613−11622.

(38) Caroff, P.; Dick, K. A.; Johansson, J.; Messing, M. E.; Deppert, K.; Samuelson, L. Controlled polytypic and twin-plane superlattices in III−V nanowires. *Nat. Nanotechnol.* **2009**, *4*, 50−55.

(39) Dick, K. A.; Thelander, C.; Samuelson, L.; Caroff, P. Crystal Phase Engineering in Single InAs Nanowires. *Nano Lett.* **2010**, *10*, 3494−3499.

(40) Algra, R. E.; Verheijen, M. A.; Borgström, M. T.; Feiner, L.-F.; Immink, G.; van Enckevort, W. J. P.; Vlieg, E.; Bakkers, E. P. A. M. Twinning superlattices in indium phosphide nanowires. *Nature* **2008**, *456*, 369−372.

(41) Burgess, T.; Breuer, S.; Caroff, P.; Wong-Leung, J.; Gao, Q.; Tan, H. H.; Jagadish, C. Twinning Superlattice Formation in GaAs Nanowires. *ACS Nano* **2013**, *7*, 8105−8114.

(42) Zhang, L.; Luo, J.-W.; Zunger, A.; Akopian, N.; Zwiller, V.; Harmand, J.-C. Wide InP Nanowires with Wurtzite/Zincblende Superlattice Segments Are Type-II whereas Narrower Nanowires Become Type-I: An Atomistic Pseudopotential Calculation. *Nano Lett.* **2010**, *10*, 4055−4060.

(43) Amato, M.; Kaewmaraya, T.; Zobelli, A.; Palummo, M.; Rurali, R. Crystal Phase Effects in Si Nanowire Polytypes and Their Homojunctions. *Nano Lett.* **2016**, *16*, 5694−5700.

(44) De Luca, M.; Fasolato, C.; Verheijen, M. A.; Ren, Y.; Swinkels, M. Y.; Kölling, S.; Bakkers, E. P. A. M.; Rurali, R.; Cartoixà, X.; Zardo, I. Phonon Engineering in Twinning Superlattice Nanowires. *Nano Lett.* **2019**, *19*, 4702−4711.

(45) Carrete, J.; López-Suárez, M.; Raya-Moreno, M.; Bochkarev, A. S.; Royo, M.; Madsen, G. K. H.; Cartoixà, X.; Mingo, N.; Rurali, R. Phonon transport across crystal-phase interfaces and twin boundaries in semiconducting nanowires. *Nanoscale* **2019**, *11*, 16007−16016.

(46) Corfdir, P.; Lewis, R. B.; Marquardt, O.; Küpers, H.; Grandal, J.; Dimakis, E.; Trampert, A.; Geelhaar, L.; Brandt, O.; Phillips, R. T. Exciton recombination at crystal-phase quantum rings in GaAs/In_xGa_{1-x}As core/multishell nanowires. *Appl. Phys. Lett.* **2016**, *109*, 082107.

(47) Royo, M.; De Luca, M.; Rurali, R.; Zardo, I. A review on III-V core-multishell nanowires: growth, properties, and applications. *J. Phys. D: Appl. Phys.* **2017**, *50*, 143001.

(48) Kresse, G.; Furthmüller, J. Efficient iterative schemes for ab initio total-energy calculations using a plane-wave basis set. *Phys. Rev. B: Condens. Matter Mater. Phys.* **1996**, *54*, 11169.

(49) Blöchl, P. E. Projector augmented-wave method. *Phys. Rev. B: Condens. Matter Mater. Phys.* **1994**, *50*, 17953.

(50) Kresse, G.; Joubert, D. From ultrasoft pseudopotentials to the projector augmented-wave method. *Phys. Rev. B: Condens. Matter Mater. Phys.* **1999**, *59*, 1758.

(51) El-Mellouhi, F.; Mousseau, N.; Ordejón, P. Sampling the diffusion paths of a neutral vacancy in silicon with quantum mechanical calculations. *Phys. Rev. B: Condens. Matter Mater. Phys.* **2004**, *70*, 205202.

(52) Sholihun; Ishii, F.; Saito, M. First-principles calculations of multivacancies in germanium. *Jpn. J. Appl. Phys.* **2016**, *55*, 011301.

(53) Amato, M.; Ossicini, S.; Canadell, E.; Rurali, R. Preferential Positioning, Stability, and Segregation of Dopants in Hexagonal Si Nanowires. *Nano Lett.* **2019**, *19*, 866−876.

(54) Amato, M.; Kaewmaraya, T.; Zobelli, A. Extrinsic Doping in Group IV Hexagonal-Diamond-Type Crystals. *J. Phys. Chem. C* **2020**, *124*, 17290−17298.

(55) Leslie, M.; Gillan, N. J. The energy and elastic dipole tensor of defects in ionic crystals calculated by the supercell method. *J. Phys. C: Solid State Phys.* **1985**, *18*, 973−982.

(56) Makov, G.; Payne, M. C. Periodic boundary conditions in ab initio calculations. *Phys. Rev. B: Condens. Matter Mater. Phys.* **1995**, *51*, 4014−4022.

(57) Freysoldt, C.; Neugebauer, J.; de Walle, C. G. V. Fully Ab Initio Finite-Size Corrections for Charged-Defect Supercell Calculations. *Phys. Rev. Lett.* **2009**, *102*, 016402.

(58) Freysoldt, C.; Neugebauer, J.; Van de Walle, C. G. Electrostatic interactions between charged defects in supercells. *Phys. Status Solidi B* **2011**, *248*, 1067−1076.

(59) Freysoldt, C.; Grabowski, B.; Hickel, T.; Neugebauer, J.; Kresse, G.; Janotti, A.; Van de Walle, C. G. First-principles

(60) Ziman, J. M. *Principles of the Theory of Solids*, 2nd ed.; Cambridge University Press, 1972; pp 37−41.

(61) Ewald, P. P. Die Berechnung optischer und elektrostatischer Gitterpotentiale. *Ann. Phys.* **1921**, *369*, 253−287.

(62) Rurali, R.; Cartoixà, X. Theory of Defects in One-Dimensional Systems: Application to Al-Catalyzed Si Nanowires. *Nano Lett.* **2009**, *9*, 975−979.

(63) Rurali, R.; Palummo, M.; Cartoixà, X. Convergence study of neutral and charged defect formation energies in Si nanowires. *Phys. Rev. B: Condens. Matter Mater. Phys.* **2010**, *81*, 235304.

(64) Zhang, S.; Northrup, J. Chemical potential dependence of defect formation energies in GaAs: Application to Ga self-diffusion. *Phys. Rev. Lett.* **1991**, *67*, 2339−2342.

(65) Northrup, J. E.; Zhang, S. B. Dopant and defect energetics: Si in GaAs. *Phys. Rev. B: Condens. Matter Mater. Phys.* **1993**, *47*, 6791− 6794.

(66) Van de Walle, C. G. Energies of various configurations of hydrogen in silicon. *Phys. Rev. B: Condens. Matter Mater. Phys.* **1994**, *49*, 4579−4585.

(67) Van de Walle, C. G.; Laks, D. B.; Neumark, G. F.; Pantelides, S. T. First-principles calculations of solubilities and doping limits: Li, Na, and N in ZnSe. *Phys. Rev. B: Condens. Matter Mater. Phys.* **1993**, *47*, 9425−9434.

(68) Luo, X.; Zhang, S. B.; Wei, S.-H. Theory of Mn supersaturation in Si and Ge. *Phys. Rev. B: Condens. Matter Mater. Phys.* **2004**, *70*, 033308.

(69) Fahey, P. M.; Griffin, P. B.; Plummer, J. D. Point defects and dopant diffusion in silicon. *Rev. Mod. Phys.* **1989**, *61*, 289−384.

(70) Stumpf, R.; Scheffler, M. Theory of self-diffusion at and growth of Al(111). *Phys. Rev. Lett.* **1994**, *72*, 254−257.

(71) Aradi, B.; Gali, A.; Deák, P.; Lowther, J. E.; Son, N. T.; Janzén, E.; Choyke, W. J. Ab initio density-functional supercell calculations of hydrogen defects in cubic SiC. *Phys. Rev. B: Condens. Matter. Phys.* **2001**, *63*, 245202.

(72) Yeh, C.-Y.; Lu, Z. W.; Froyen, S.; Zunger, A. Zinc-blende− wurtzite polytypism in semiconductors. *Phys. Rev. B: Condens. Matter Mater. Phys.* **1992**, *46*, 10086−10097.

(73) Ito, T. Simple Criterion for Wurtzite-Zinc-Blende Polytypism in Semiconductors. *Jpn. J. Appl. Phys., Part 1* **1998**, *37*, L1217−L1220.

(74) García, A.; Cohen, M. L. First-principles ionicity scales. I. Charge asymmetry in the solid state. *Phys. Rev. B: Condens. Matter Mater. Phys.* **1993**, *47*, 4215−4220.

(75) García, A.; Cohen, M. L. First-principles ionicity scales. II. Structural coordinates from atomic calculations. *Phys. Rev. B: Condens. Matter Mater. Phys.* **1993**, *47*, 4221−4225.

(76) Abu-Farsakh, H.; Qteish, A. Ionicity scale based on the centers of maximally localized Wannier functions. *Phys. Rev. B: Condens. Matter Mater. Phys.* **2007**, *75*, 085201.

(77) Wei, S.-H.; Zunger, A. Predicted band-gap pressure coefficients of all diamond and zinc-blende semiconductors: Chemical trends. *Phys. Rev. B: Condens. Matter Mater. Phys.* **1999**, *60*, 5404−5411.

(78) Yeh, C.-Y.; Wei, S.-H.; Zunger, A. Relationships between the band gaps of the zinc-blende and wurtzite modifications of semiconductors. *Phys. Rev. B: Condens. Matter Mater. Phys.* **1994**, *50*, 2715−2718.

(79) Lany, S.; Zunger, A. Assessment of correction methods for the band-gap problem and for finite-size effects in supercell defect calculations: Case studies for ZnO and GaAs. *Phys. Rev. B: Condens. Matter Mater. Phys.* **2008**, *78*, 235104.

(80) Giorgi, G.; Schilfgaarde, M.; Korkin, A.; Yamashita, K. On the Chemical Origin of the Gap Bowing in (GaAs)$_{1-x}$Ge$_{2x}$ Alloys: A Combined DFT-QSGW Study. *Nanoscale Res. Lett.* **2010**, *5*, 469− 477.

(81) Ley, L.; Pollak, R. A.; McFeely, F. R.; Kowalczyk, S. P.; Shirley, D. A. Total valence-band densities of states of III-V and II-VI compounds from x-ray photoemission spectroscopy. *Phys. Rev. B: Solid State* **1974**, *9*, 600−621.

(82) Lautenschlager, P.; Garriga, M.; Logothetidis, S.; Cardona, M. Interband critical points of GaAs and their temperature dependence. *Phys. Rev. B: Condens. Matter Mater. Phys.* **1987**, *35*, 9174−9189.

(83) Zanolli, Z.; Fuchs, F.; Furthmüller, J.; von Barth, U.; Bechstedt, F. Model GW band structure of InAs and GaAs in the wurtzite phase. *Phys. Rev. B: Condens. Matter Mater. Phys.* **2007**, *75*, 245121.

(84) Zanolli, Z. Private communication.

(85) Tedeschi, D.; De Luca, M.; del Águila, A. G.; Gao, Q.; Ambrosio, G.; Capizzi, M.; Tan, H. H.; Christianen, P. C. M.; Jagadish, C.; Polimeni, A. Value and anisotropy of the electron and hole mass in pure wurtzite InP nanowires. *Nano Lett.* **2016**, *16*, 6213− 6221.

(86) Mishra, A.; Titova, L. V.; Hoang, T. B.; Jackson, H. E.; Smith, L. M.; Yarrison-Rice, J. M.; Kim, Y.; Joyce, H. J.; Gao, Q.; Tan, H. H.; Jagadish, C. Polarization and temperature dependence of photo-luminescence from zincblende and wurtzite InP nanowires. *Appl. Phys. Lett.* **2007**, *91*, 263104.

(87) Belabbes, A.; Panse, C.; Furthmüller, J.; Bechstedt, F. Electronic bands of III-V semiconductor polytypes and their alignment. *Phys. Rev. B: Condens. Matter Mater. Phys.* **2012**, *86*, 075208.

(88) Belabbes, A.; Bechstedt, F. Forbidden Band-Edge Excitons of Wurtzite-GaP: A Theoretical View. *Phys. Status Solidi B* **2019**, *256*, 1800238.

(89) Giorgi, G.; Yamashita, K. Amphoteric behavior of Ge in GaAs: an LDA analysis. *Modell. Simul. Mater. Sci. Eng.* **2011**, *19*, 035001.

(90) Galicka, M.; Buczko, R.; Kacman, P. Segregation of Impurities in GaAs and InAs Nanowires. *J. Phys. Chem. C* **2013**, *117*, 20361− 20370.

(91) Diao, Y.; Liu, L.; Xia, S. Exploration the p-type doping mechanism of GaAs nanowires from first-principles study. *Phys. Lett. A* **2019**, *383*, 202−209.

(92) Du, Y. A.; Sakong, S.; Kratzer, P. As vacancies, Ga antisites, and Au impurities in zinc blende and wurtzite GaAs nanowire segments from first principles. *Phys. Rev. B: Condens. Matter Mater. Phys.* **2013**, *87*, 075308.

(93) Coutinho, J.; Torres, V. J. B.; Jones, R.; Briddon, P. R. Electrical activity of chalcogen-hydrogen defects in silicon. *Phys. Rev. B: Condens. Matter Mater. Phys.* **2003**, *67*, 035205.

(94) Alkauskas, A.; Broqvist, P.; Pasquarello, A. Defect Energy Levels in Density Functional Calculations: Alignment and Band Gap Problem. *Phys. Rev. Lett.* **2008**, *101*, 046405.

(95) Komsa, H.-P.; Broqvist, P.; Pasquarello, A. Alignment of defect levels and band edges through hybrid functionals: Effect of screening in the exchange term. *Phys. Rev. B: Condens. Matter Mater. Phys.* **2010**, *81*, 205118.

(96) Alkauskas, A.; Pasquarello, A. Band-edge problem in the theoretical determination of defect energy levels: The O vacancy in ZnO as a benchmark case. *Phys. Rev. B: Condens. Matter Mater. Phys.* **2011**, *84*, 125206.

(97) Graham, A. M.; Corfdir, P.; Heiss, M.; Conesa-Boj, S.; Uccelli, E.; Fontcuberta i Morral, A.; Phillips, R. T. Exciton localization mechanisms in wurtzite/zinc-blende GaAs nanowires. *Phys. Rev. B: Condens. Matter Mater. Phys.* **2013**, *87*, 125304.

(98) De Luca, M.; Rubini, S.; Felici, M.; Meaney, A.; Christianen, P. C. M.; Martelli, F.; Polimeni, A. Addressing the Fundamental Electronic Properties of Wurtzite GaAs Nanowires by High-Field Magneto-Photoluminescence Spectroscopy. *Nano Lett.* **2017**, *17*, 6540−6547.